Phys. Status Solidi A, 1–6 (2012) / **DOI** 10.1002/pssa.201127596

physica status solidi a
www.pss-a.com
applications and materials science

Deep centers in a $CuInGaSe_2$/CdS/ZnO:B solar cell

In-Hwan Choi*[,1], Chul-Hwan Choi[2], and Joo-Won Lee[2]

[1] Department of Physics, Chung-Ang University, Seoul 156-756, Korea
[2] LG Innotek, Gyeonggi-do, Ansan-si 426-791, Korea

Received 6 October 2011, revised 7 February 2012, accepted 28 February 2012
Published online 21 March 2012

Keywords CIGS solar cells, deep centers, deep-level transient spectroscopy, electron-beam induced currents

* Corresponding author: e-mail ihchoi@cau.ac.kr, Phone: +82-2-820-5193, Fax: +82-2-817-8876

$CuInGaSe_2$(CIGS)/CdS/ZnO:B heterojunction solar cells and CIGS/Al Schottky junction diodes were fabricated, and the defect centers were examined by capacitance–voltage (*C–V*) measurements and deep-level transient spectroscopy (DLTS). The homogeneity of the junction in the CIGS heterojunction solar cell was examined by electron-beam induced current (EBIC) measurements. The distribution of the defect concentrations in the CIGS absorber layer of the CIGS/CdS/ZnO:B heterojunction changed remarkably with depth. On the other hand, the defect distribution in the CIGS layer of the CIGS Schottky junction was quasi-homogeneous. One electron and one hole trap were observed from CIGS Schottky junction, whereas one electron trap and two hole traps were found in the CIGS/CdS/ZnO:B heterojunction.

1 Introduction Thin-film solar cell technology is a promising alterative to monocrystalline and polycrystalline silicon solar cell technology, which are both popular in the solar cell market today. In particular, copper indium gallium diselenide ($CuInGaSe_2$ or CIGS) has become one of the leaders in thin-film solar cells. Recently, in fact, a CIGS/CdS/ZnO thin-film solar cell with a 19.9% conversion efficiency and an 81.2% fill factor was reported by the National Renewable Energy Laboratory (NREL) [1]. Moreover, since CIGS solar cells have shown long-term stability in the field, they have become quite attractive for industrial applications.

To increase the energy conversion efficiency of a CIGS-based solar cell, it is important to fully understand the junction properties and the deep trap centers that act as recombination centers and can cause a decrease in the short-circuit current. By analyzing the electron beam-induced currents (EBIC) and junction capacitance, researchers have been able to study the junction properties that affect the electrical characteristics of heterojunction solar cells. For example, EBIC analysis has been employed to investigate the shape and strength of the electric field built in the depletion region of p–n or Schottky junction semiconductor devices. Additionally, recent studies have examined the carrier collection properties and the influence of the interface on CIGS solar cells by EBIC cells [2, 3]. Moreover, deep-level transient spectroscopy (DLTS) is a useful measurement technique for examining the electrical defect states formed near the junction interface. In fact, Bhattacharya et al. characterized the defect states formed in CIGS solar cells using DLTS measurements. They first fabricated CIGS solar cells using three different methods – solution-based electroplated precursors, auto-plated precursors, and physical vapor deposition – and then they compared the different defect states between each method [4]. Abushama et al. [5] also examined the capacitance–voltage (*C–V*) and DLTS properties of CIGS solar cells prepared with different compositions of absorber layers ranging from Cu-rich to In-rich. In both studies, the authors discussed their DLTS results based on the assumption that the CIGS/CdS/ZnO heterojunction solar cells were composed of a one-sided step junction, such as an n^+p junction. The CIGS/CdS/ZnO solar cell, however, cannot be a strictly one-sided junction because of the existing CdS buffer and because of the formation of a buried junction in the CIGS layer. The real location of a p–n junction is believed to be in the CIGS layer since the Cd atoms diffuse from the CdS buffer layer into the CIGS absorber layer. Therefore, to understand the deep centers that are formed in the CIGS solar cells more clearly, a comparison the deep centers of a CIGS/CdS/ZnO heterojunction to a Schottky junction (e.g., p-type CIGS/Al) is needed.

In this study, a CIGS absorber layer was prepared using a three-step co-evaporation method while the Schottky

junction diodes were prepared simply by thermal vacuum deposition of Al onto CIGS thin films. CIGS solar cells were fabricated by the sequential deposition of CdS and boron-doped ZnO. To compare the defect states formed in the CIGS absorber layer and CIGS solar cell, the junction properties of the CIGS/CdS/ZnO:B solar cells and the CIGS/Al Schottky junction diodes were examined by *C–V*, EBIC, and DLTS measurements.

2 Experimental details Cu-poor CIGS absorber layers were prepared using a co-evaporation method with the following three-step process: (i) the formation of an $(In,Ga)_2Se_3$ layer on Mo-coated soda-lime glass substrates heated to 350 °C, followed by (ii) the deposition of Cu and Se at approximately 550 °C, and (iii) the addition of more In, Ga, and Se at the same substrate temperature. CIGS solar cells were then fabricated by the sequential deposition of a CdS buffer layer, using the chemical bath deposition (CBD) method, and a boron-doped ZnO window layer, using metal-organic chemical vapor deposition (MOCVD). The CIGS/Al Schottky junction diode, on the other hand, was prepared by thermal vacuum deposition of an Al metal onto CIGS thin films. The thicknesses of the CIGS absorber layer, the CdS buffer layer, and the ZnO window layer were 2.2 μm, 50 nm, and 0.8 μm, respectively. The confirmed composition ratios [Cu]/[III], [Ga]/[III], and [I + III]/[2VI] of the CIGS absorber layer were approximately 0.93, 0.37, and 0.97, respectively, as measured by X-ray fluorescence (XRF). The properties near the depletion region in both the CIGS/CdS/ZnO:B solar cells and the CIGS/Al Schottky junction diodes were examined by *C–V*, EBIC, and DLTS measurements.

The DLTS equipment consisted of a Boonton 72BD capacitance meter (1 MHz test signal) and a National Instruments data acquisition system (with a built-in analog-to-digital converter and a pulse generator in the PC card). All measurements were carried out in the dark, and the scanning temperature ranged from LN_2 temperature to room temperature. The pulse and reverse bias voltages applied to the diode were −0.5 and −1 V, respectively. Although the period was 40 ms, the duration of a single pulse was 4 ms. The transient capacitance was acquired every $t^n = 0.05^n$ ms after each pulse, where $n = 1, 2, 3 \ldots 10$. *C–V* measurements were carried out using the same capacitance meter and data acquisition system of the DLTS analysis at room temperature. The variation range of bias voltages were $0 \sim -2$ V for the CIGS/CdS/ZnO:B solar cell and $0.5 \sim -2$ V for the CIGS/Al Schottky diode. The test frequency was 1 MHz.

The EBIC and cross-sectional images of the CIGS/CdS/ZnO:B heterojunction solar cells were obtained via a scanning electron microscope (SEM). The EBIC and SEM images were obtained at an electron beam voltage of 20 kV.

3 Results and discussion

3.1 EBIC image Figure 1a shows a cross-sectional SEM image for the Mo/CIGS/CdS/ZnO:B solar cell fabricated on a soda-lime glass substrate, and Fig. 1b displays its EBIC image. The EBIC image in Fig. 1b is a map of the short-circuit current of the photovoltaic (PV) device induced by the scanning electron beam that was injected in the direction normal to the cross-sectional image. The brighter region in the EBIC image of Fig. 1b indicates a higher induced current in the device by the electron beam. Each point in Fig. 1a corresponds to a point in Fig. 1b, and the intersections on both Fig. 1a and b indicate the highest EBIC generating locations in the figure.

As shown in Fig. 1, the brightest points in the EBIC image appear not at the interface of the junction but in the middle of the CIGS absorber layer. In principle, the EBIC peaks in a heterojunction diode shift toward the side of the lower energy band gap with respect to the actual electrical junction of the device because the carrier-pair generating ratio by the primary beam of electrons is inversely proportional to the energy expended by the incident electron.

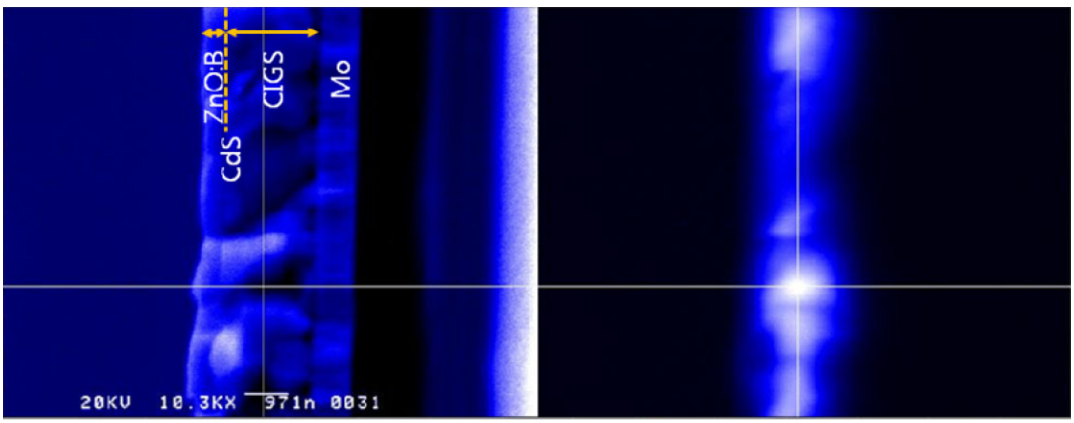

Figure 1 (online color at: www.pss-a.com) (a) SEM cross-sectional image of a CIGS/CdS/ZnO:B heterojunction solar cell, and (b) its electron-beam induced current (EBIC) image created by mapping the change in the electron-beam induced short-circuit current with a scanning electron beam along the device cross-section.

The expended energy scales directly with the band gap of the material and is one of the characteristic constants of the material [6]. Consequently, the electron–hole pair generation rate should decrease as the scanning electron beam approaches the CdS from the CIGS, causing the EBIC signal to appear as a shifted peak away from the CdS. Moreover, this shifting effect could also be caused by the p–n junction forming in the middle of CIGS absorber layer. Since the cation atoms in the II–VI compounds, i.e., Cd and Zn in the buffer and window layers, can easily diffuse into the CIGS absorber layer and then form donor impurity states, the actual electrical junction position should not be at the interface of the CdS and CIGS but should be at the middle of the CIGS absorber layer instead. Some studies [7] have suggested that, since the CdS buffer layer in CIGS solar cells is not sufficiently thick to form a CdS crystal lattice or a well-defined band gap, the CdS buffer layer in CIGS solar cells can only be a surface passivation layer. Likewise, other studies have suggested that the rectifying interface is a buried homo-junction within the CIGS absorber layer [8].

In ordinary, the EBIC image spread more widely than the shape of the actual electric field formed in the depletion region because the carrier generation depth varied with the electron beam acceleration voltages [9]. Although the peak position shifted and spread with respect to both the actual position and the shape of the electric field formed in the depletion region, as mentioned above, the EBIC signal provided important information regarding the built-in electric field in the junction device.

Even though the energy conversion efficiency of the CIGS solar cells used in this experiment was as high as 17.4% ($V_{oc} = 667$ mV, $I_{sc} = 39.7$ mA/cm^2, and FF = 65.4%), non-homogenous EBIC signals were observed, as shown in Fig. 1b. These signals may be due to various types of physical non-uniformities, which can produce variations in the local photo-voltage and shunting. Since the equivalent circuit for a single diode can be represented with a network of many diodes, which may be individually defined, any infinitesimal non-uniform point in a solar cell can be caused by decreasing the shunt resistance. Consequently, it decreases the total current generated by the device. Therefore the preparation of more homogenous CIGS films is an important step to increasing the conversion efficiency of CIGS solar cells.

3.2 *C–V* curves Capacitance–voltage measurements are a useful characterization technique for an abrupt junction device. A plot of the inverse square depletion capacitance per unit area, $1/C_d{}^2$, as a function of the bias voltage for an ideal abrupt junction device with a constant space–charge density is straightforward, i.e.,

$$\left(\frac{1}{C_d^2}\right) = B(V_b - V_a),$$

where B is the inclination and V_b is the intercept of the voltage axis at $y = 0$ $\left(1/C_d^2 = 0\right)$. For a one-sided abrupt junction, such as a Schottky or n$^+$p junction, the inclination of B becomes $2/\varepsilon_s qN$. For the more general case of a one-sided abrupt junction with a variable doping density according to depth, the space-charge density, $\rho(x) = qN(x)$, according to the location of the depletion edge (as a function of DC bias), can be determined from the derivative of the C–V graph, i.e., $\mathrm{d}(1/C_d^2)/\mathrm{d}V_a$. Figure 2 and its inset show plots of $1/C_d^2$ as function of V_a and the depth profile of carrier concentration, respectively, at room temperature, which were obtained from the CIGS/CdS/ZnO:B heterojunction and the CIGS/Al Schottky diode. As shown in the Fig. 2 inset, the carrier concentration obtained from the CIGS/Al Schottky junction diode had a nearly constant value with an increasing reverse bias, $-V_a$, whereas those values for the CIGS heterojunction cell had a concave shape with a minimum point at a 0.7 μm depth from the junction interface. This result indicates that the space-charge density in the depletion region of the CIGS heterojunction cell varied with the depletion-edge location. On the other hand, the CIGS/Al Schottky junction had an almost constant space-charge density regardless of the depletion-edge location. The equivalent circuit for a CIGS/CdS/ZnO:B heterojunction can be assumed to be a series of two distinctive capacitors. In contrast, the equivalent circuit for a CIGS/Al Schottky junction is a capacitor. In a CIGS heterojunction, one of the capacitors (C_{CdS}) is formed by a CdS intrinsic buffer layer, while the other capacitor (C_{CIGS}) is formed by depletion in the CIGS absorber layer. Therefore, the total capacitance of a CIGS heterojunction, C_{cell}, can be expressed as $C_{cell} = C_{CIGS} \times C_{CdS}/(C_{CIGS} + C_{CdS})$. Under a reverse bias, C_{CdS} is constant, whereas C_{CIGS} varies as function of the reverse bias. Moreover, a CIGS/CdS/ZnO:B solar cell is not strictly a one-sided abrupt junction.

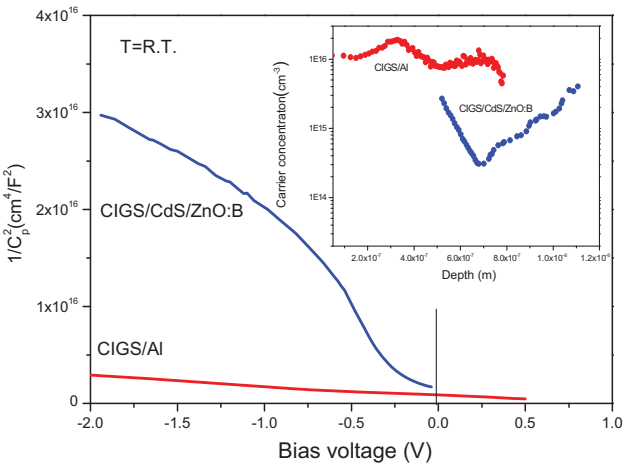

Figure 2 (online color at: www.pss-a.com) Junction capacitance of a CIGS/CdS/ZnO:B solar cell and a CIGS/Al Schottky junction diode as a function of the bias voltage at room temperature in the dark. The inset in this figure shows the change in carrier concentration according to the depth, which is related to the applied reverse bias voltage.

From the C–V measurements of the Schottky junction diode, the distribution of the defect concentration in this sample along the depth was found to be quasi-homogeneous, and the estimated carrier concentration was approximately $1 \times 10^{16}\,cm^{-3}$. In the case of the CIGS/CdS/ZnO:B heterojunction, the defect concentrations varied remarkably between 3×10^{14} and $5 \times 10^{15}\,cm^{-3}$ within the applied bias region. The results were analyzed assuming that the CIGS/CdS/ZnO:B solar cell was a one-sided abrupt junction. This variation in the impurity concentration near the interface of CIGS/CdS was due to the inter-diffusion of some foreign impurities, such as Cd from CdS, during the continued sequence process. Then, the substitution of Cd atoms with Cu vacancies, Cd_{Cu}, formed donor states that compensated for the acceptor impurities, V_{Cu}, in the CIGS. This compensation is why the defect concentration in the CIGS heterojunction near the interface was less than that of the CIGS Schottky diode.

3.3 DLTS spectrum Deep-level transient spectroscopy is used widely to observe the non-radiative deep-trap centers that cannot be observed by photoluminescence. DLTS is a high-frequency capacitance technique that employs the transitional phenomenon of returning from a non-equilibrium state to an equilibrium state. It provides information on the activation energy, trap cross-section, and trap density of the impurity levels formed in the Schottky barrier or depletion region of a p–n junction.

Figure 3a and b shows the DLTS measurements obtained from a CIGS/Al Schottky junction and a CIGS/CdS/ZnO:B heterojunction, respectively. The capacitance transients were observed just after the pulse (−0.5 V) returned to the reverse bias (−1 V), and were measured every $t^n = 0.05^n$ ms, where n is an integer, as a function of the temperature. Figure 3a shows the variations of $\Delta C_{ij} = C(t_i) - C(t_j)$ with temperature, where the time ratio of t_i/t_j is 16. The peaks with negative values in Fig. 3a are due to the hole emission (electron capture) from the majority-carrier hole trap, whereas the peaks with positive values are due to the electron emission (hole capture) from the minority-carrier electron trap. The DLTS spectrum in Fig. 3b was obtained from the CIGS/CdS/ZnO:B heterojunction diode under the same conditions that Fig. 3a was obtained from the CIGS/Al Schottky junction diode.

An electron trap (denoted by A in Fig. 3a and Fig. 4) and a hole trap (denoted by B in Fig. 3a and Fig. 4) were observed in the CIGS/Al Schottky junction sample. The activation energies of the hole and electron traps were 440 and 73 meV, respectively. The capture cross-sections of the electron, σ_n, and hole, σ_p, were 1.27×10^{-14} and $4.60 \times 10^{-19}\,cm^2$, respectively.

In the CIGS/CdS/ZnO:B sample, three trap levels were observed. One was the electron trap (denoted by C in Fig. 3b and Fig. 4), and two were hole traps (denoted by D and E in Fig. 3b and Fig. 4). The activation energy of the electron trap C was approximately 8.4 meV, and the electron capture cross-section, σ_n, was $2.2 \times 10^{-20}\,cm^2$. The activation

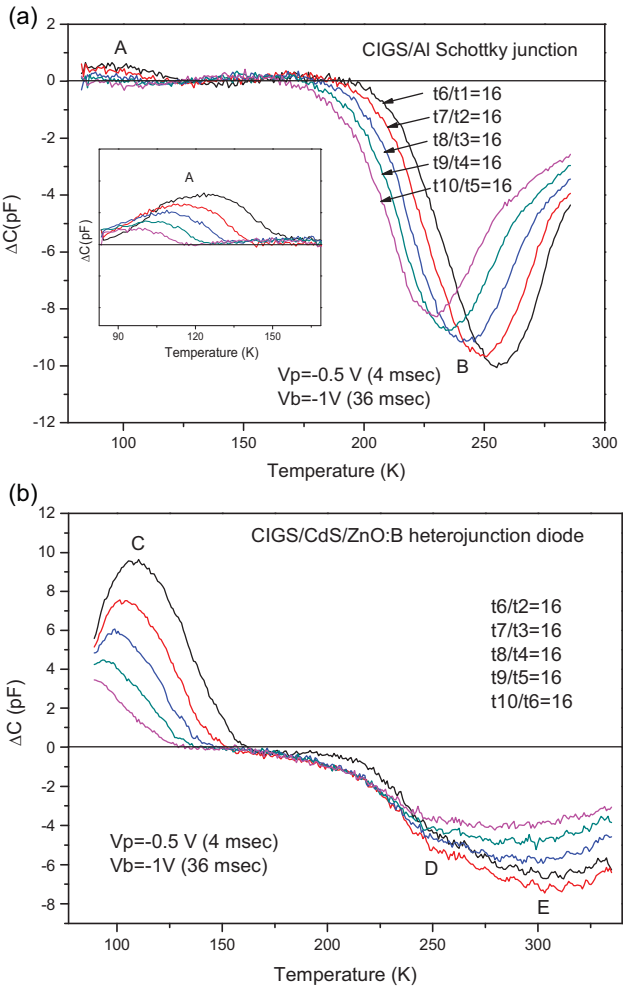

Figure 3 (online color at: www.pss-a.com) DLTS spectra of the (a) CIGS/Al Schottky junction and (b) CIGS/CdS/ZnO:B heterojunction solar cell.

energies of the two holes traps (D and E) could not be resolved, but the hole trap D appears to be the same as the previously mentioned hole trap B in Fig. 3a. The majority-carrier trap peak, located near 230 K, was observed in both samples. The minority-carrier trap peaks, A and C, located near 80 K in both samples, had different activation energies, and the intensity of peak C was much stronger than that of peak A. The majority-carrier trap peak E, which appeared to have larger activation energy than trap B (or D), was observed near room temperature. This additional broad DLTS peak (E) is presumed to have originated from the interface states, and the origin of the majority trap D was estimated to be the same as trap B.

A p-type CIGS semiconductor forms an ohmic contact with Mo metal, whose work function is 4.6 eV. On the contrary, it forms a Schottky contact with Al metal, whose work function is 4.28 eV. Thus, a Mo/p-CIGS/Al metal junction forms a one-side Schottky junction that forms a depletion region just beneath the Al metal electrode toward the CIGS side. On the other hand, the p–n junction in the

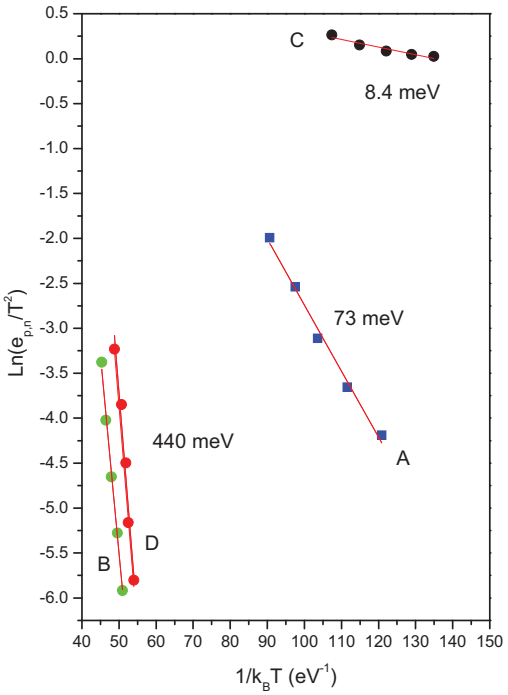

Figure 4 (online color at: www.pss-a.com) Plot of $\ln(1/\tau_m T^2)$ as a function of $1/kT$ for the CIGS/Al Schottky junction and the CIGS/CdS/ZnO:Al heterojunction.

CIGS/CdS/ZnO solar cell was mostly formed on the inside of the CIGS absorber layer instead of at the interface of CIGS/CdS. The depletion region spread from the CdS layer to the middle of the CIGS layer, as indicated in the EBIC image. The depletion region in the CIGS heterojunction was then extended in both directions – toward the CIGS and the CdS – under a reverse bias. Consequently, it is expected that all the results obtained from the CIGS/CdS/ZnO:B sample originated from both the CIGS absorber and the CdS buffer layer. The deep majority (acceptor) carrier trap, which had an activation energy of 440 meV and was observed on both samples, may have been created in response to the introduction of foreign impurities, such as the Fe contained in the Cu precursor. The Fe^{2+} atoms that filled the In sites acted as acceptors with activation energies of ~400 meV [10–12].

The defect formation energy in a CIS chalcopyrite semiconductor was calculated by Zhang et al. [13], who used first-principle calculations for the defect energies. They found that the defect formation energies were not fixed constants, but varied considerably – both with the position of the Fermi level and with the chemical potential of the atomic species. According to their results, the order of formation energies in p-type Cu-poor and In-rich CIS semiconductors is $V_{Cu} < In_{Cu} < V_{In} < Cu_{In} < Cu_i$ [13]. Thus, the most probable intrinsic point defects are V_{Cu} and In_{Cu} in our samples. While In_{Cu} formed a donor level, V_{Cu} formed an acceptor level in the CIGS. Therefore, the deep minority (donor) carrier trap, which was found in the CIGS/Al Schottky junction and had an activation energy of 73 meV, may have been created in response to the In atoms that filled the Cu sites (i.e., In_{Cu}). The observation of a donor level having an ionization energy of 60–80 meV in CIS semiconductors has been reported by many researchers [14, 15]. Some authors in these reports argue that the presence of this level is due to a Se vacancy [16, 17], V_{Se}, but we believe that the probability of this vacancy is very low because the absorbers used in this experiment were Se-rich. Moreover, a minority (donor) carrier trap, which was found in the CIGS/CdS/ZnO:B Schottky junction and had activation energy of 8.4 meV, may have been due to the Cd atoms that filled the Cu sites (i.e., Cd_{Cu}). This conjecture is supported by the fact that the Cd atoms in the CdS buffer layer can easily diffuse into the CIGS absorber layer during the window deposition process, thereby creating Cd_{Cu} defects.

4 Conclusion The junction properties of a CIGS/CdS/ZnO:B heterojunction solar cell and a CIGS/Al Schottky junction were examined by *C–V*, EBIC, and DLTS measurements. Non-homogenous EBIC signals were observed, even in the relatively high-performance PV devices that had an energy conversion efficiency of 17.4%.

Although the defect distribution estimated by the *C–V* measurement of the grown CIGS sample along the depth was quasi-homogeneous, the defect concentration in the solar cell prepared by the same absorber varied remarkably. The estimated carrier concentration of the CIGS absorber was approximately $1 \times 10^{16}\,cm^{-3}$, and the defect concentrations of the CIGS heterojunction varied from 3×10^{14} to $5 \times 10^{15}\,cm^{-3}$ within the applied bias region due to the interdiffusion of Cd from CdS.

In the DLTS measurement of the CIGS/Al Schottky junction, we found one minority- and one majority-carrier trap. The activation energies of the hole and electron traps in the CIGS cell were 440 and 73 meV, respectively. From the CIGS/CdS/ZnO:B heterojunction, a minority-carrier trap and more than two majority-carrier traps were observed. The activation energy of the majority-carrier traps was 8.4 meV.

The deep majority (acceptor) carrier trap, which had activation energy of 440 meV, may have been formed in response to the introduction of a foreign impurity, such as the Fe contained in the Cu precursor element. Likewise, the deep minority (donor) carrier trap with an activation energy of 73 meV might have been created in response to the In atoms that filled the Cu sites (i.e., In_{Cu}), and the minority (donor) carrier trap with an activation energy of 8.4 meV may have been due to the Cd atoms that were substituted into the Cu sites (i.e., Cd_{Cu}).

Acknowledgements This work was supported by the New & Renewable Energy of the Korea Institute of Energy Technology Evaluation and Planning (KETEP) grant funded by the Ministry of Knowledge Economy, Republic of Korea (2008NPV12P150000).

References

[1] I. Repins, M. A. Conteras, B. Egaas, C. DeHart, J. Scharf, C. L. Perkins, B. To, and R. Noufi, Prog. Photovolt.: Res. Appl. **16**, 235 (2008).

[2] R. Kniese, M. Powalla, and U. Rau, Thin Solid Films **515**, 6163 (2007).
[3] M. J. Romero, M. M. Al-Jassim, R. G. Dhere, F. S. Hasoon, M. A. Contreras, T. A. Gessert, and H. R. Moutinho, Prog. Photovolt.: Res. Appl. **10**, 445 (2002).
[4] R. N. Bhattacharya, A. Balcioglu, and K. Ramanathan, Thin Solid Films **384**, 65 (2001).
[5] J. Abushama, S. Johnston, R. Ahrenkiel, and R. Noufi, Deep level transient spectroscopy and capacitance–voltage measurements of Cu(In,Ga)Se_2, Photovoltaic Specialists conference, 19–24 May 2002; Conference record of the 29th IEEE, pp. 740–743.
[6] R. J. Matson, R. Noufi, R. K. Ahrenkiel, R. C. Powell, and D. Cahen, Sol. Cells **16**, 495. (1986).
[7] B. Canava, J. Vigneron, A. Etcheberry, D. Guimard, P. P. Grand, F. J. Guillemoles, D. Lincot, S. Ould Saad Hamartly, Z. Djebbour, and D. Mencaraglia, Thin Solid Films **289**, 431 (2003).
[8] I. M. Dharmadasa, Semicond. Sci. Technol. **24**, 055016 (2009).
[9] J. I. Goldstein, D. E. Newberry, P. Echlin, D. C. Joy, C. Fiori, and E. Lifshin, Scanning Electron Microscopy and X-ray Microanalysis (Plenum Press, New York, 1981), pp. 53–102.
[10] H. Neumann, E. Nowak, and G. Kühn, Cryst. Res. Technol. **16**, 1369 (1981).
[11] H. J. von Bardeleben, J. Appl. Phys. **56**, 321 (1984).
[12] H. Neumann, E. Nowak, G. Kühn, and B. Heise, Thin Solid Films **102**, 201 (1983).
[13] S. B. Zhang, S. H. Wei, and A. Zunger, Phys. Rev. B **57**, 9642 (1998).
[14] H. Neumann, R. D. Tomlinson, N. Avgerino, and E. Nowak, Phys. Status Solidi A **75**, K199 (1983).
[15] J. J. M. Binsma, L. J. Giling, and J. Bloem, J. Lumin. **27**, 35 (1982).
[16] P. Migliorato, J. L. Shay, H. M. Kasper, and S. Wagner, J. Appl. Phys. **46**, 1777 (1975).
[17] G. Masse and E. Redjai, J. Appl. Phys. **56**, 1154 (1984).

